International Forum on Aeroelasticity and Structural Dynamics
IFASD 2024
17-21 June 2024, The Hague, The Netherlands

NEW DESIGN OF WHIRL FLUTTER AEROELASTIC DEMONSTRATOR

Jiří Čečrdle[1*], Ondřej Vích[1], Jan Stárek[1], Jarmil Vlach[1], Martin Kolář[1], Miroslav Šmíd[1]

[1] Czech Aerospace Research Centre (VZLU), Prague, Czechia
[*]cecrdle@vzlu.cz

Keywords: Aeroelastic experiment, Whirl Flutter, W-WING, OFELIA Project

Abstract: This paper presents the new design of aeroelastic demonstrator for the experimental research into whirl flutter aeroelastic phenomenon. The demonstrator was adapted from the former aeroelastic model of a commuter aircraft for 40 passengers. It represents a half-wing with the span of 2.56 m with the nacelle and powered propeller (radius 0.35 m). In the frame of the previous project, two experimental campaigns were accomplished in 2014 and 2015. For the further usage of the demonstrator, the modifications and upgrades were proposed. This paper presents the preparatory activities including the demonstrator design, instrumentation, and aerodynamic and structural analyses. Two experimental campaigns are planned in 2024 including the measurements of aerodynamic derivatives and measurements of dynamic response and whirl flutter stability. The results will be used for verification of the computational tools and analytical models in the frame of the OFELIA project that is aimed at development of the new open fan-based power plant system utilized for a new generation short-medium range turboprop aircraft.

1 INTRODUCTION

Whirl flutter may appear on turboprop aircraft due to the effect of rotating parts, such as a propeller or a gas turbine engine rotor. It is driven by motion-induced unsteady aerodynamic propeller forces and moments acting at the propeller plane. Rotating mass generates additional forces and moments, and rotating propeller also cause an aerodynamic interference effect between a nacelle and a wing. Whirl flutter may cause unstable vibration, even a failure of an engine suspension or an entire wing. The phenomenon was analytically discovered by Taylor and Browne in 1938 [1]. In 1945, Ribner set the basic formulae for the aerodynamic derivatives of propeller forces and moments due to the motion and velocities in pitch and yaw [2, 3]. The importance of the whirl flutter phenomenon on practical applications was recognized after the accidents of two Lockheed L-188 C Electra II airliners in 1959 and 1960 [4].

The physical principle of whirl flutter is complicated and analytical solution of the propeller aerodynamic forces is unreliable. Further, whirl flutter is extremely sensitive to structural damping. Therefore, validation of the analytically obtained results by means of experiments on aeroelastic models is required. The important experiments were carried out in NASA LARC by Reed, Bennett, Kvaternik and many others [5 - 10]. Experimental research into whirl flutter was also carried out in NAL [11]. A comprehensive description of both past and current experimental research into whirl flutter is provided in [12].

VZLU aeroelastic workgroup has been focused on experimental aeroelasticity since fifties. The past activities included aeroelastic wind tunnel testing in the frame of the Czech aircraft structures certification. Many experiments of various aircraft were carried out. The used aeroelastic models are currently often rebuilt, and utilized as research demonstrators for investigation of novel concepts, systems, methods, etc. An example of such a utilization is the subjected demonstrator that represents the half-wing and engine of a typical commuter turboprop aircraft structure. The nacelle structure is variable, there are three options available: 1) The nacelle with engine attachment with four degrees-of-freedom, 2) The nacelle with a nonlinear attachment of the engine in pitch and nonlinear aileron actuation [13, 14] and finally 3) The nacelle with a powered rotating propeller for investigation of the whirl flutter phenomenon (W-WING) [15 - 17].

2 WHIRL FLUTTER AEROELASTIC DEMONSTRATOR

The demonstrator was adapted from a former aeroelastic model of the commuter aircraft for 40 passengers. It consists of a half-wing (span: 2.56 m) with the nacelle, engine, and propeller. The structural parameters may be considered realistic for the subjected aircraft category. The total mass of the model is approximately 55 kg (wing 30 kg and nacelle 25 kg). Two experimental campaigns have been accomplished so far in the frame of the previous project. Further measurements are planned in the frame of the current OFELIA project. For the purpose of the further experiments, design modifications and other upgrades of the demonstrator were proposed. The main change is the installation of the new motor with the sufficient power. Also, additional sensors and equipment are installed. Contrary to the past measurements that included the response measurements only, the planned experiments will also include measurements of the propeller aerodynamic derivatives. For this purpose, special sting-mounted variant, i.e., propeller-nacelle only (W-STING) was proposed. Finally, the complex system of steady and unsteady flow field measurement was proposed for the dynamic response measurements. Figure 1 shows the unmodified state of the demonstrator.

Figure 1: Unmodified variant of W-WING aeroelastic demonstrator.

Structural characteristics of the wing and aileron are modelled by a duralumin spar of variable cross-section and by lead weights. The aerodynamic shape is covered with modular balsa and plastic segments. The wing is fixed at the root to the pylon that is attached to the wind tunnel manipulator. The aileron is actuated by the electromagnetic shaker placed at the wing root via a push-pull rod. Other choices of actuation include an active control system capable of simulating

the additional mass, damping or stiffness terms. The system allows to introduce non-linear characteristics of these terms.

Changeable parameters include those main ones influencing the whirl flutter. The nacelle model has two degrees of freedom (engine pitch and yaw). The stiffness parameters are modeled by means of cross-spring pivots and the stiffness parameters can be adjusted independently by replacing the spring leaves with the thickness ranging from 2.2 to 3.5 mm. In addition, both pivots are independently movable in the direction of the propeller axis to adjust the pivot points of both vibration modes. The distance between the front and rear stations of both pivots is roughly 0.15 m. Overall length of the nacelle and the propeller position remains unchanged. Nacelle includes the movable weight to adjust the moment of inertia and the center of gravity of the engine system. The weight may be also used to preserve the center of gravity position in case the pivot stations change. The gyroscopic effect of the rotating mass is simulated by the mass of the propeller blades. The propeller diameter is 0.7 m, the geometry represents scaled-down real 5-blade Avia V-518 propeller. The propeller blades are adjustable at a standstill. Two sets of blades with the diverse mass (made of duralumin and steel) are available. Finally, the wing dynamic characteristics may be adjusted using weights that formerly simulated the wing fuel.

3 PROPELLER AERODYNAMIC FORCE ANALYSIS

During the past tests, the selection of the motor was done assuming the propeller operation near the zero-thrust condition, and therefore, the required power was relatively low, and the low-power motor was installed. Obviously, for the operation of the propeller near the zero-thrust condition, the operational slot for a specific blade angle of attack was limited in terms of the airflow velocity. However, during the past tests, such an operation was found as ineffective as this operation slot was found as too narrow and the frequent changes in the blade angles of attack with the interruption of the test to re-adjust the blades were necessary.

To avoid this practice, demonstrator is newly equipped with the powerplant system with the sufficient power to operate as much as possible without limitations in terms of the airflow velocities and propeller revolutions. Such power plant enables to provide the test with the real thrusted propeller. The fixed rpm thrusted mode of the propeller rotation is now applicable for evaluation of the thrust influence on the whirl flutter stability. This is the main advantage compared to the typical practice of the windmilling propeller usage.

To predict the necessary power of the motor and operational margins of the propeller in terms of the revolutions and airflow velocities, the analytical study of the propeller aerodynamic forces was performed. The analyses were aimed at determining the areas of the propeller operation modes (thrust, reversal, zero-thrust and generator). The analytical method was based on the CFD solver of the full NS equations for a viscous compressible flow based on the finite volume method. The rotating domain of 1/5 cylinder with the periodic condition was used. Solution included fully parallelized K-ω SST turbulence model with variable CFL. The total number of elements was approximately 40 mil. The volume grid was hybrid with the unstructured hex elements around the viscous walls of the blade passing through pyramids into volumetric tetra elements. The propeller surface grid included quad elements. The example of the CFD computational domain including the propeller blade tip is shown in figure 2.

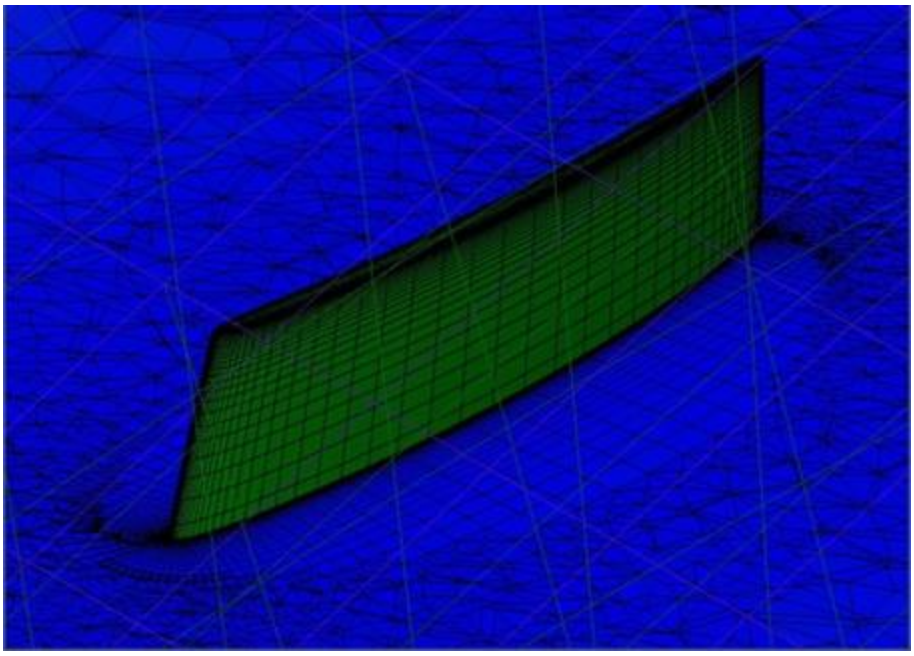

Figure 2: CFD computational domain around the blade tip.

The evaluated parameters included the propeller revolutions (600 to 5000 rpm), airflow velocity (10 to 40 m/s) and the blade angle of attack (-5 to 15 deg, measured at 75 % of blade radius). The examples of results are shown in figures 3 (required power vs. advance ratio) and 4 (propeller thrust vs. advance ratio).

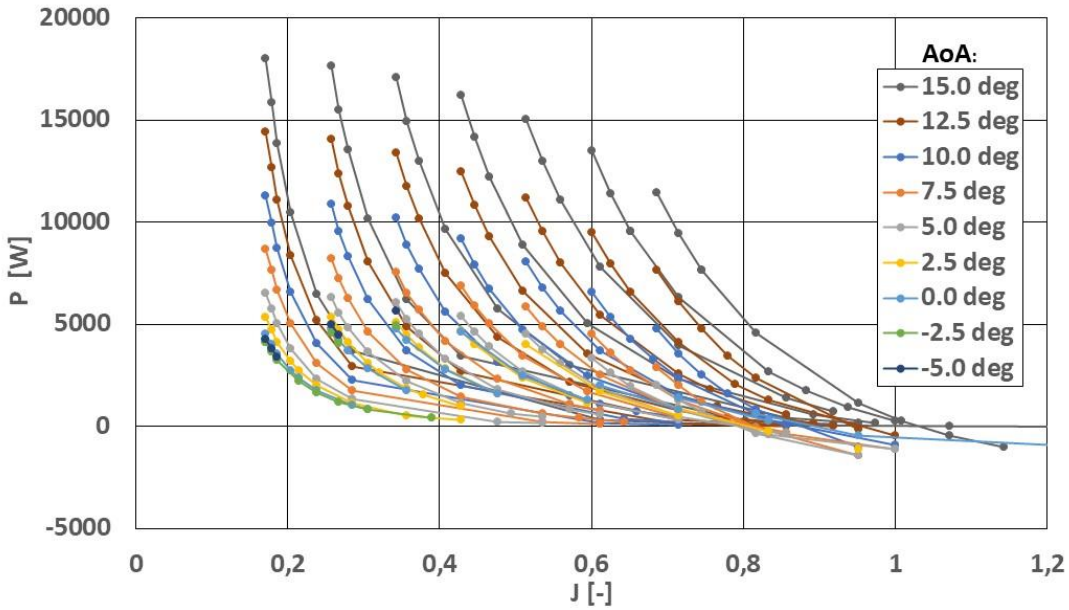

Figure 3: Propeller aerodynamic force analysis, power vs. advance ratio.

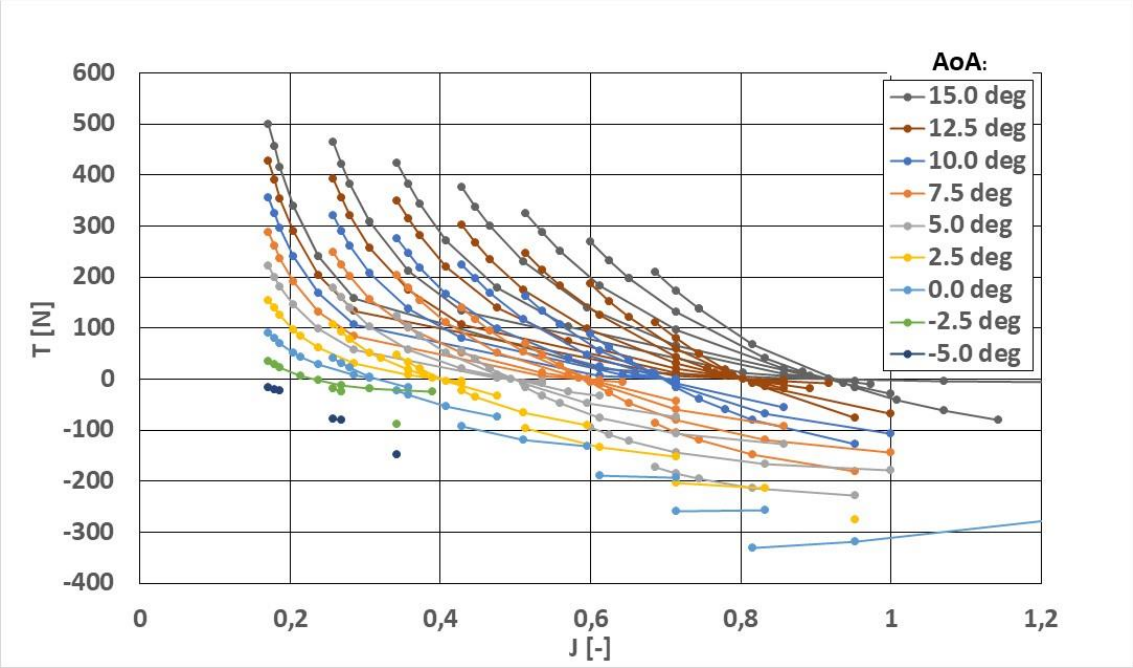

Figure 4: Propeller aerodynamic force analysis, thrust vs. advance ratio.

The selection of the appropriate motor was based on the results of analyses, and on further limitations (mass, dimensions etc.). The selected type is NOVA 15-50 WK motor with the nominal power of 15 kW. Considering the practical operation during the wind tunnel tests, the expected available operational power is 10 – 11 kW. It is obvious that the selection was the technical compromise including the request to obtain the maximal power, but at the same time, to preserve the acceptable mass and dimensions. The operational envelope of the motor is therefore limited by the available power. Table 1 shows the example of the operational envelope for the propeller blade angle-of-attack of 12.5 deg. The applicable regimes, i.e., propeller is in the thrust mode with the sufficient power, are the green cells while the red cells represent the regimes of the propeller in the thrust mode with the insufficient power and yellow and brown cells represent the regimes of the propeller in the reversal mode. The numbers represent corresponding propeller thrust.

Table 1 – Propeller thrust and operational envelope (green cells), blade AoA 12.5 deg.

Blade angle	12.5	V [m/s]						
	T (N)	10	15	20	25	30	35	40
RPM	200							
	400							
	600							
	800							
	1000	-2.0						
	1200	5.1						
	1400		-8.7					
	1600		0.6					
	1800		11.4					
	2000			-8.2				
	2200			5.6				
	2400			20.1	-19.2			
	2600				-3.9			
	2800				12.2			
	3000	132.8	106.6	73.6	31.6	-18.4	-67.5	
	3200							
	3400					21.1		
	3600	203.8	174.9	139.2	97.6	44.1	-13.9	-75.4
	3800						7.4	
	4000							
	4200	288.7	257.0	218.9	174.9	124.4	60.0	-8.4
	4400							18.4
	4600	354.1	321.1	280.9	234.5	182.4	120.7	49.3
	4800	389.5	355.8	314.6	266.9	213.7	152.8	79.6
	5000	426.5	392.0	348.9	301.0	246.9	185.9	111.7

4 NACELLE DESIGN

The nacelle was completely redesigned, particularly in the front part. Motor was replaced by the more powerful, water-cooled, and larger one and the connection with the propeller was redesigned. A new thrust metering load cell was designed respecting the allocated space between the motor console and the rest of the structure and the required range. The upper sliding beam in the front part was replaced with a new, flat-section beam. Also, the sliding weight compensating for the displacements of cross springs was redesigned and the root part of the nacelle was reinforced.

For the W-STING option, blocking devices for both pitch and yaw degrees-of-freedom were created. Blocking is applied onto a single (either pitch or yaw) degree-of-freedom during the

measurement of aerodynamic derivatives. This is achieved without the necessity of cross-spring pivots changing. Such an approach significantly reduces manipulation time and increases the effectiveness of the measurement. Also, new supports for the cross-spring leaves integrating attachment points for blocking devices were designed. Finally, connection to the six-component balance was designed.

The shape of the fairing was slightly changed and the new upper fairing covering the complete shape of the nacelle was designed for W-STING. The design is documented in the following figures. Figure 5 shows the design model with the description of the main parts. Figure 6 shows the same depiction, but with the pitch and yaw blocking installed. Blocking devices are the parts covering the cross-spring pivots. Finally, figure 7 shows the covered nacelle for W-WING variant. The following figures demonstrate specific, newly designed details: Propeller attachment (figure 8), thrust measurement cell and sliding weight (figure 9), motor attachment (figure 10) and the upper beam (figure 11).

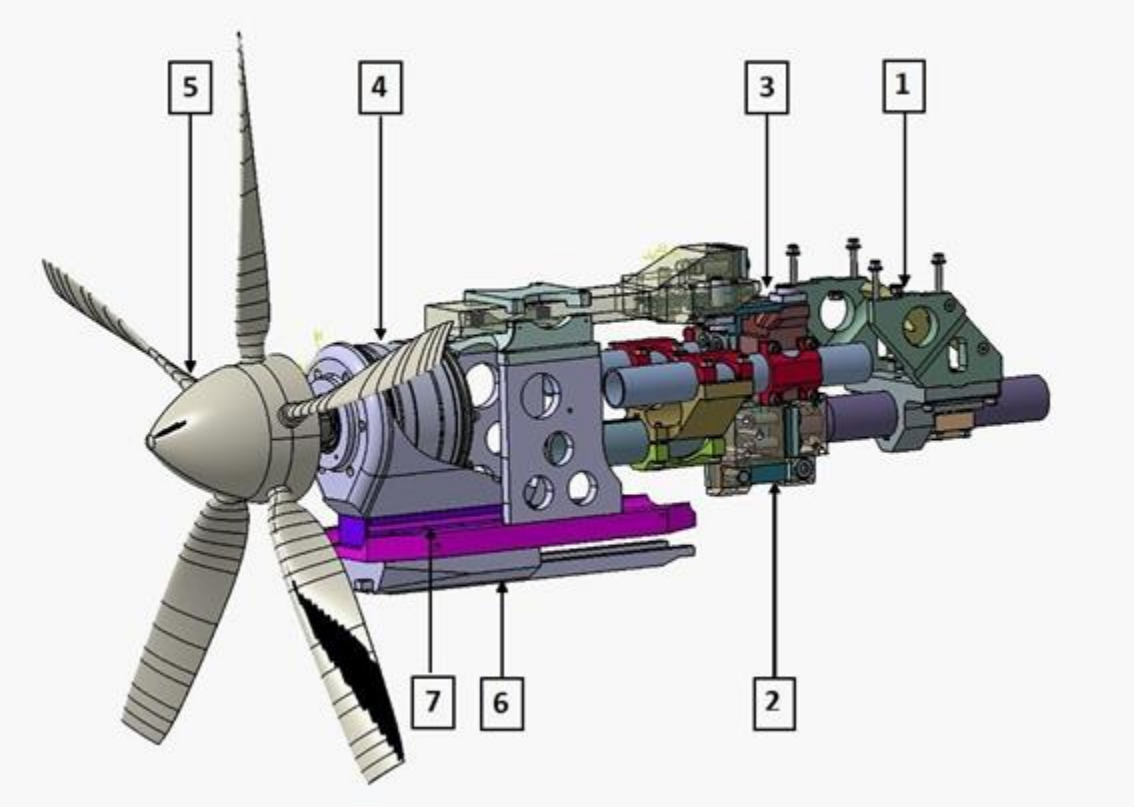

Figure 5: New design, uncovered nacelle: (1) Wing mounting, (2) Yaw attachment, (3) Pitch attachment, (4) Motor, (5) Propeller, (6) Movable weight, (7) Thrust measurement cell.

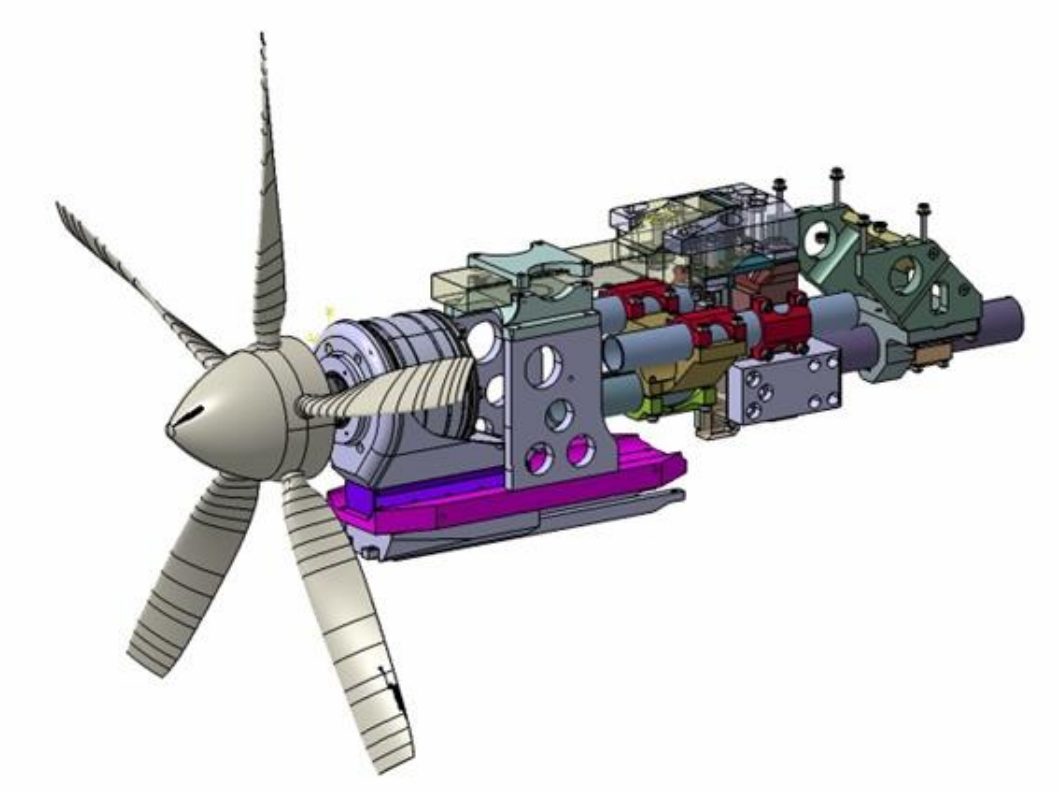

Figure 6: New design, uncovered nacelle with installed blocking of pitch and yaw movement.

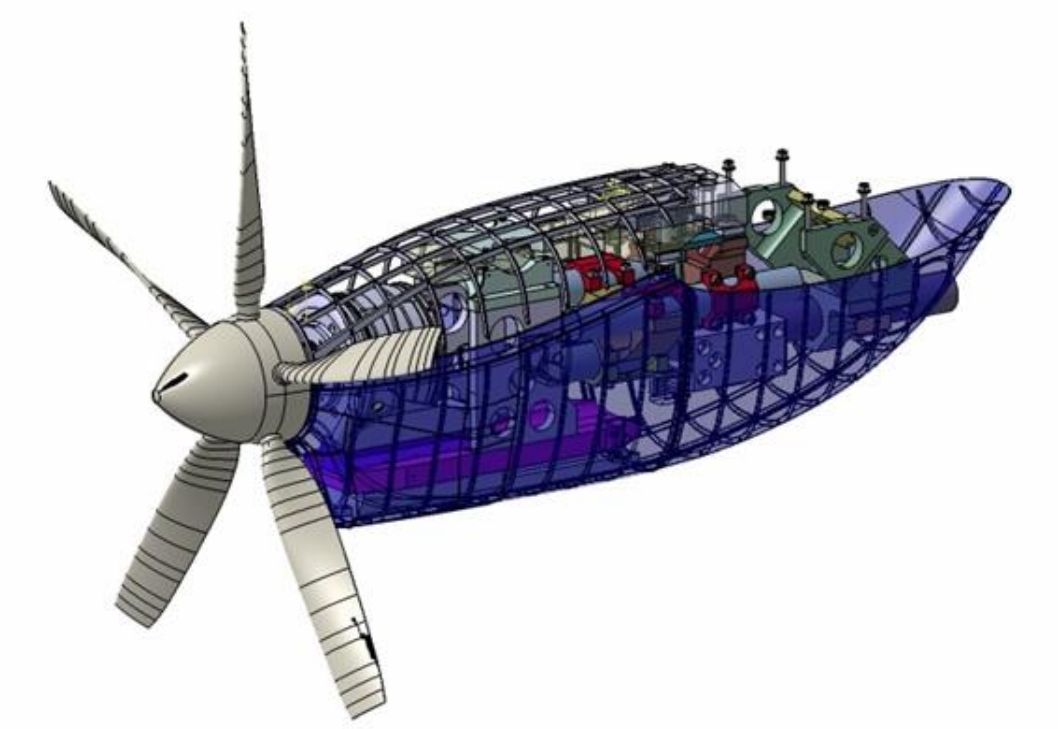

Figure 7: New design, covered nacelle, W-WING option.

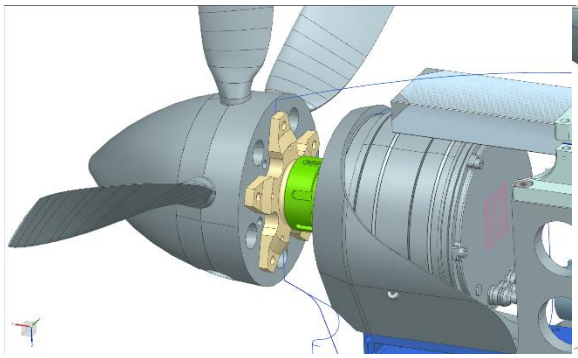

Figure 8: Propeller attachment.

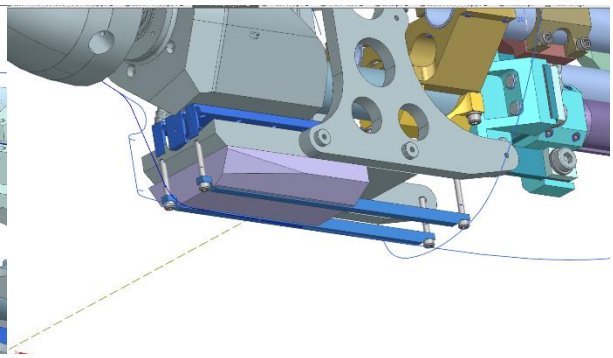

Figure 9: Thrust measurement cell and sliding weight.

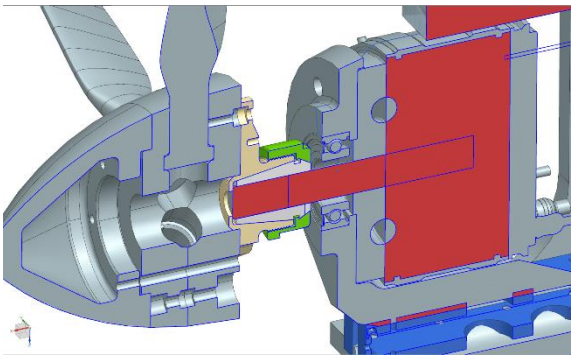

Figure 10: Motor attachment.

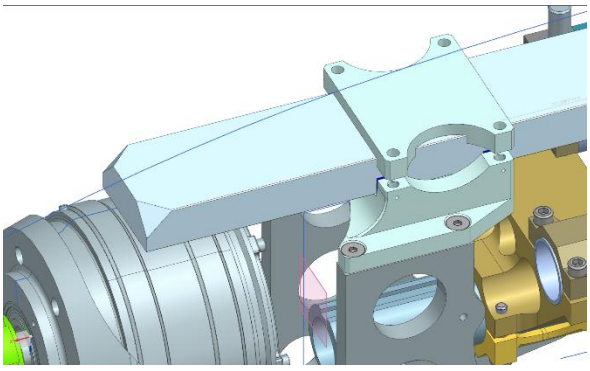

Figure 11: Upper beam design.

5 STRENGTH CHECKS

The appropriate strength checks of the newly designed structural parts and assemblies were performed by means of FEM. Calculations included:

1) Stress analyses of cross-spring pivots and other parts of the assembly. Applied load included aerodynamic load generated by the propeller and the weight load. Analyses included all variants of pitch and yaw cross-spring pivots (in terms of thickness). In addition, the analysis of the state with locked pitch and yaw degrees-of-freedom were performed. Safety criteria were determined. The minimal safety ratio towards the yield stress was 1.45 ($k_{Rp0.2}$ = 1.45). Figure 12 shows the example of the static deformation of the complete assembly. The nacelle incidence may vary between 5 and 10 deg, depending on the thickness of spring leaves. Static deformation is then compensated by means of the special wedge-shaped washers placed under the leaves of the pitch spring attachment. Each set of leaves has the specific set of washers. This compensation eliminates the static deformation theoretically to zero, in practice, some small deformation remains. Figures 13 and 14 show the examples of stress maps on the lower beam and on the spring leaves.

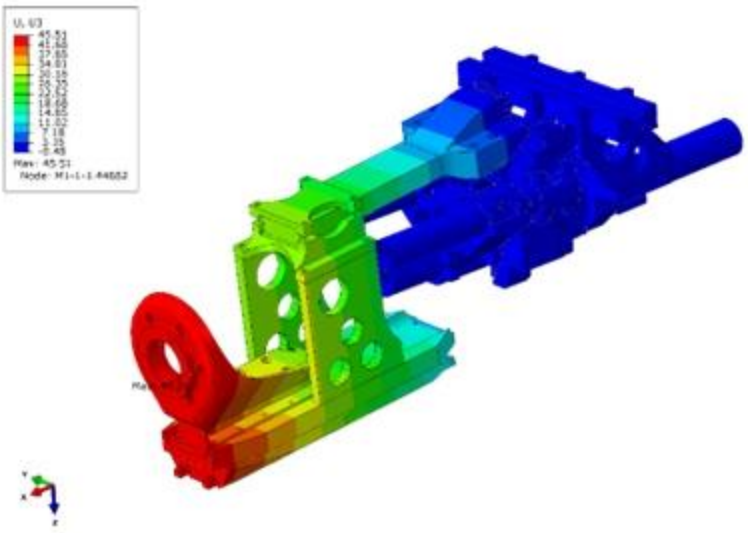

Figure 12: Example of nacelle assembly deformation.

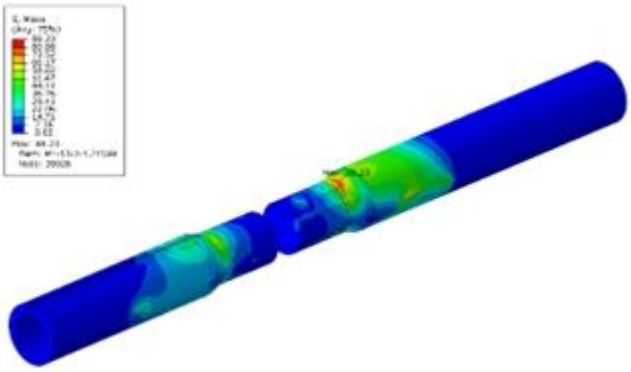

Figure 13: Lower beam, strength analysis, example of stress map.

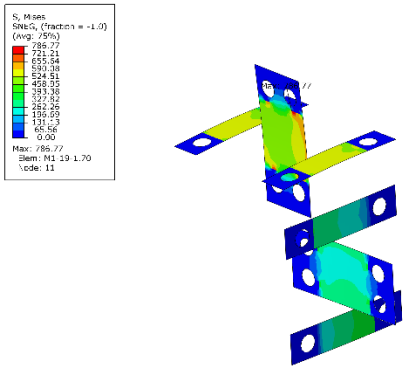

Figure 14: Cross-spring pivot leaves, strength analysis, example of stress map.

2) Thrust measurement cell analysis. Analyses included several load cases. The minimal safety ratio towards the yield stress was 2.3 ($k_{Rp0.2}$ = 2.3). Figure 15 shows the example of the stress map.

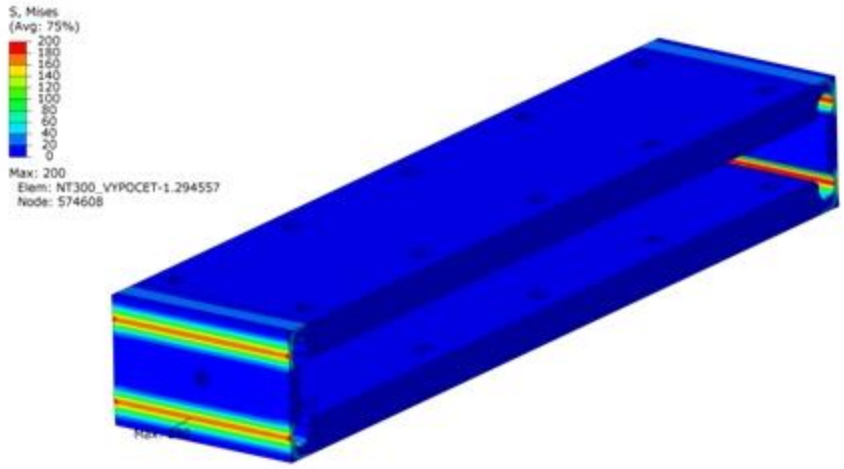

Figure 15: Thrust measurement cell, strength analysis, example of stress map.

3) Propeller blade attachment and propeller shaft strength check with respect to the propeller aerodynamic forces and centrifugal forces. Calculations included front and rear part of the propeller boss and the propeller blade mounting. Maximal applicable propeller revolutions with respect to centrifugal forces was determined at 5500 rpm considering the safety ratio towards the yield stress of 2.0 ($k_{Rp0.2}$ = 2.0). Figure 16 shows the example of the stress map.

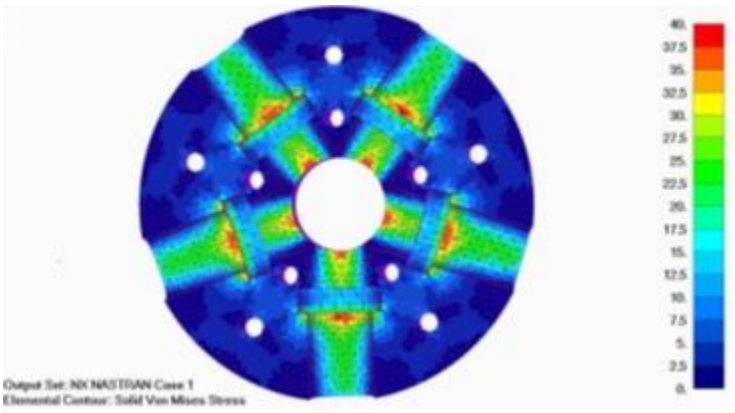

Figure 16: Front part of propeller boss, stress map, duralumin blades.

4) Propeller blade modal analysis. The purpose was to evidence the "rigidity" of the blade. The results showed the frequency of the first mode (1st bending mode) at 106.8 Hz (steel blade) and at 108.1 Hz (duralumin blade). Such figures are sufficiently high to consider the blade as rigid. Figure 17 shows the shape of the 1st bending mode.

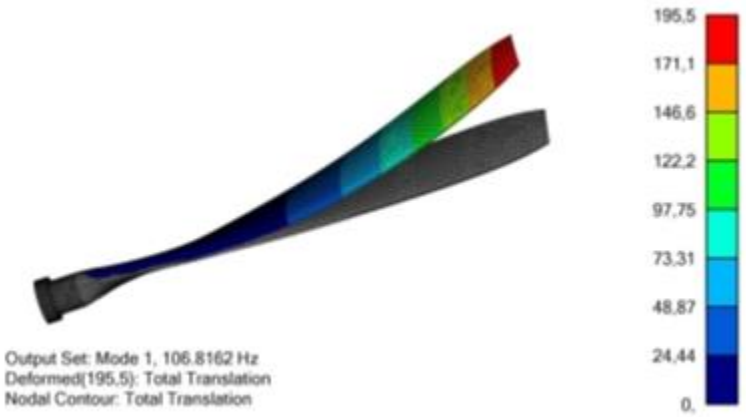

Figure 17: Blade 1st bending mode.

5) Further analyses that included modal analysis of the variant with pitch and yaw blocking to evidence the "rigidity" and stress checks of the nacelle-to-wing (sting) connecting bolts were performed.

6 DEMONSTRATOR INSTRUMENTATION

1) Strain gauges: Sensors are placed in the root and half-span sections to measure the vertical bending, in-plane bending, and torsional deformations as shown in figure 18.

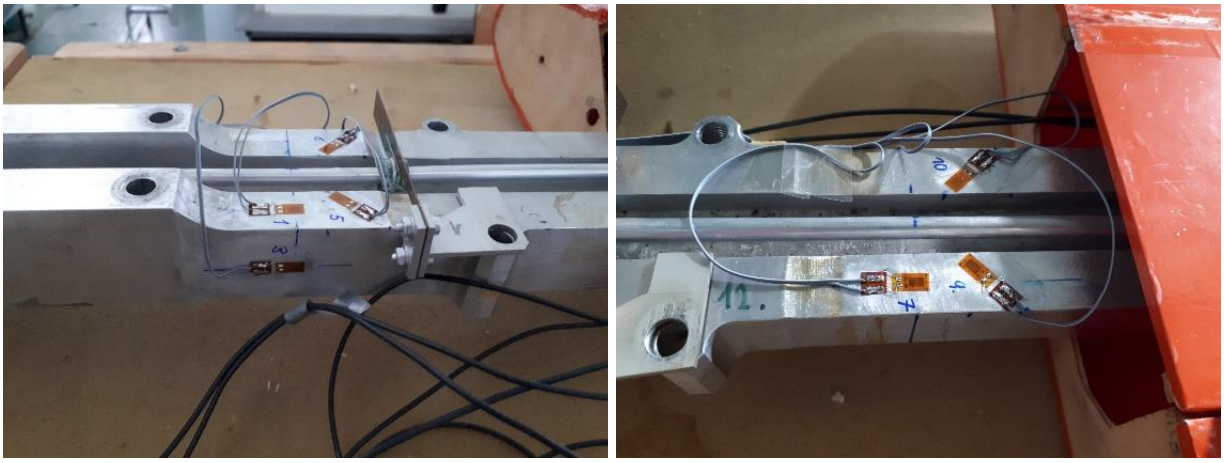

Figure 18: Strain gauges, wing root and half-span sections.

2) Accelerometers: Wing is instrumented at six spanwise sections and two positions chordwise for the vertical direction and at a single position in the wingtip for the longitudinal direction. Nacelle is instrumented in two sections (front and rear) for both vertical and horizontal directions and at the rear section also for the longitudinal direction. The demonstrator is equipped with 18 uniaxial sensors in total. The installation of the wing accelerometers is shown in figure 19.

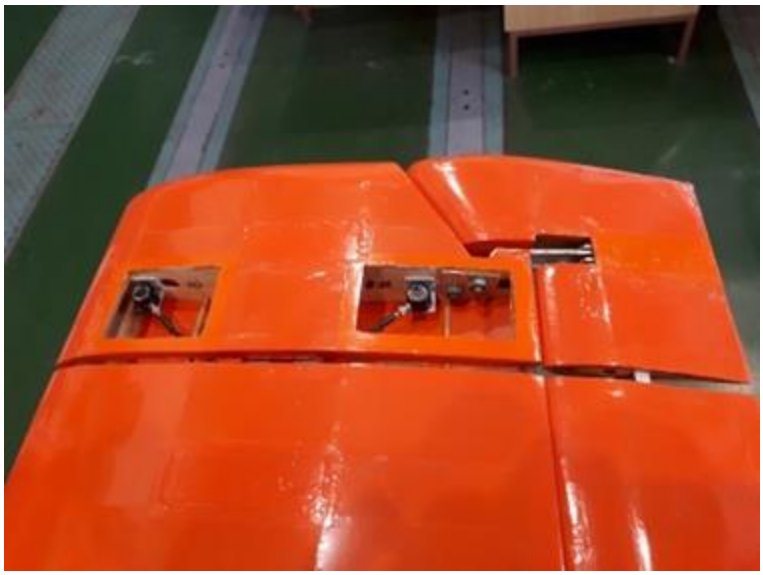

Figure 19: Wing accelerometers installation (wingtip section).

3) Propeller and motor-related sensors: The motor is equipped with the servo amplifier to manage and evaluate propeller revolutions, torque, and immediate power. In addition, independent rpm sensor is also installed. Propeller thrust is measured using the balance cell.

4) Excitation system: Demonstrator is equipped with the system of aerodynamic excitation by aileron flapping. Aileron is actuated via push-pull rod using an electromagnetic shaker placed behind the splitter plate. Push-pull rod is instrumented with the deflection sensor for evaluation of aileron angular deflection and as a safety guard to prevent damage of the shaker and rod. Excitation system includes various signals, such as harmonic, sweep or impulse.

5) Measurement of aerodynamic derivatives: Pitch and yaw hinge moments are measured using six-component balance (see figure 20). Pitch and yaw angles are measured using strain gauges installed onto spring leaves (see figure 21). Also, wind tunnel manipulator angle is registered.

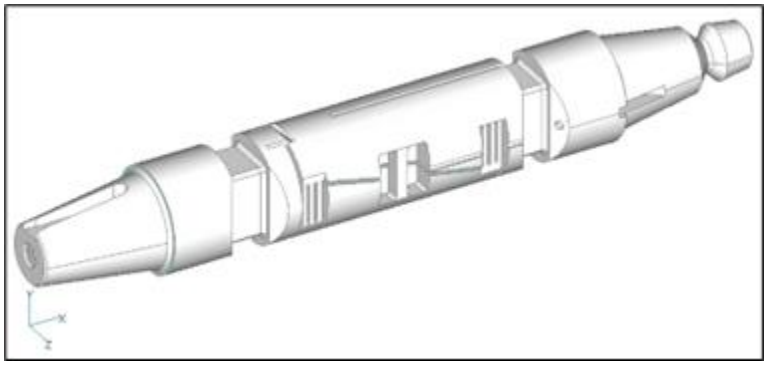

Figure 20: Six-component balance for measurement of pitch and yaw moments.

Figure 21: Strain gauges for measurement of pitch and yaw deformation angles.

6) Aerodynamic flow field measurements: The aerodynamic flow field measurement includes both steady and unsteady aero measurements. It gives pressure and velocity data on several points of the flow field. Steady measurement includes 15 points in total while unsteady measurement includes 17 points in total. Acquisition will be done one location at a time. Sensors include Aeroprobe, L-shaped five-hole fast response 1kHz and Wire probe for CTA Dantec Streamline anemometer. Aft mounted installation of sensors is demonstrated in figure 22.

Figure 22: Installation system for flow field sensors.

7) LabVIEW-based application: Special in-house LabVIEW-based application is used for management of the test, data acquisition and processing. The application is used to control the propeller rotation (constant or controlled rate ramp) and to manage the aerodynamic excitation by the aileron flapping (harmonic constant, harmonic sweep, impulse). The same application is also used for the calibration of sensors. The program also provides the immediate power and propeller revolutions signal from which the torque of the propeller is evaluated. Finally, the

application provides a safeguard preventing the destruction of the demonstrator, provided the response at the critical points (nacelle front section and wingtip section) exceeds the preselected threshold, by turning off the propeller motor, the wind tunnel fan and, provided used, turning off the aerodynamic excitation by the aileron. The "slow" data, such as propeller revolutions and airflow velocity are stored at a sampling frequency of 2 Hz, while the real-time data from the strain-gauges and selected accelerometers are stored at a sampling frequency of 2 kHz. The data are depicted in the time domain as well as pre-processed into the form of the power spectral densities. The main GUI window of the application is shown in figure 23.

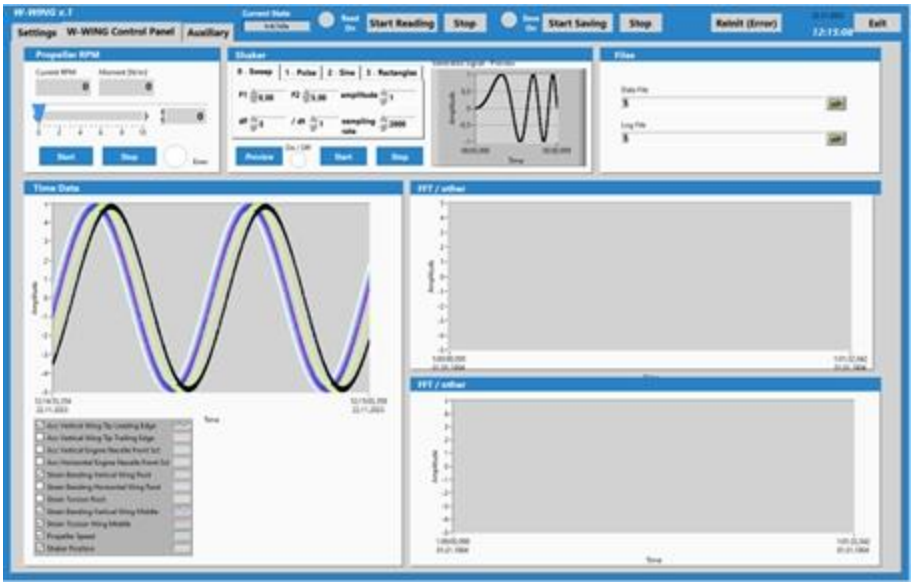

Figure 23: LabVIEW-based application, main GUI window.

8) LMS TestLab system: Apart from the above-mentioned application, the LMS TestLab system is used. The system acquires the continuous signals from all accelerometers and the airflow velocity signal. The amplitude evolution of the frequency components corresponding to the engine whirl motion is monitored in real-time. The data are then used for the assessment of the demonstrator vibration response using the methods of FFT and OMA.

7 OUTLOOK

The planned future activities include ground tests and wind tunnel tests of the demonstrator.

Ground test activities are aimed at determining the structural parameters. First, the nacelle component model testing that includes stiffness measurement for all choices of spring leaves and the modal tests for all choices of spring leaves and both propellers is planned. The gained results include pitch and yaw effective stiffness parameters and natural frequencies for all measured configurations. Next, the complete model modal testing is planned. The tests include standard GVT (without propeller rotation) covering wing modes and engine modes for a single configuration. The gained results include complete set of modal parameters, i.e., natural frequency, mode shape, modal mass, and damping ratio for the mentioned modes. Further, the OMA tests with the rotating propeller at several rpm levels are planned. These tests include propeller at two choices of the propeller blade angle of attack and mass equivalent disc. The gained results include

natural frequencies and mode shapes. The purpose is to evaluate the influence of the propeller aerodynamic force and gyroscopic effect on the modal parameters. The experiment with the mass equivalent disc is aimed at separating the influence of the gyroscopic effect.

Wind tunnel tests include two measurement campaigns. The first one includes measurement of propeller aerodynamic derivatives using the sting-mounted model (W-STING) and measurement of the dynamic responses and flutter stability using wing-mounted model (W-WING). The second campaign is then focused on the dynamic response measurement only. Contrary to the first one, it also includes the aerodynamic flow field measurements.

8 CONCLUSION

The paper describes the mechanical concept and preparatory activities related to the aeroelastic demonstrator for experimental investigation into whirl flutter phenomenon. Two variants are prepared: 1) Sting-mounted nacelle with pitch and yaw degrees of freedom, motor, and powered propeller (W-STING) aimed at measuring of the propeller aerodynamic derivatives and 2) Wing-mounted nacelle that include also complete wing modes (W-WING) that is aimed at measuring of the dynamic responses and flutter stability states. The concept of the nacelle allows adjusting of all main parameters influencing whirl flutter.

A broad testing campaign in the VZLU 3m-diameter wind tunnel is planned. The test schedule includes the measurements of propeller aerodynamic derivatives, dynamic response and whirl flutter stability measurements and aerodynamic flow field measurements. Structural characteristics will be checked by stiffness tests and modal tests. The experimental results will be subsequently utilized for verification of the analytical models and computational tools [19, 20] that will be used for development of the new power plant system, characterized as an open-fan concept, utilized for a new generation short-medium range turboprop aircraft.

ACKNOWLEDGEMENT

Program and topic: HORIZON-JU-CLEAN-AVIATION-2022-01-SMR-01, Ultra Efficient Propulsion Systems for Short and Short-Medium Range Aircraft. Project nr. and title: 101102011, Open Fan for Environmental Low Impact of Aviation (OFELIA).

Other contributing people of the VZLU project team: Petr Vrchota, Miloš Javůrek, Zuzana Lašová, Miloš Chvátal, Miroslav Golda, Robert Kulhánek, Jan Raška, Petr Malínek, Václav Klouda and Radek Doubrava.

REFERENCES

[1] Taylor, E. S., and Browne, K. A. Vibration Isolation of Aircraft Power Plants, *J. Aerosp. Sci*., 1938, *6(2):43-49*.

[2] Ribner, H. S. Propellers in Yaw, *NACA, Report 820*, 1945.

[3] Ribner, H. S. Formulas for Propellers in Yaw and Charts of the Side - Force Derivatives, *NACA, Report 819*, 1945.

[4] Donham, R. E. and Watts, G. A. Whirl Flutter First Case, *In: The Revolution in Structural Dynamics*, (Editor Dr. Hugh Flomenhoft), Dynaflo Press, Palm Beach Gardens, FL, USA, 99-109, 1997.

[5] Reed, W. H. and Bland, S. R. An Analytical Treatment of Aircraft Propeller Precession Instability, *NASA, TN D-659*, 1961.

[6] Reed, W. H. and Bennett, R. M. Propeller Whirl Flutter Considerations for V/STOL Aircraft, *In: CAL/TRECOM Symposium*, Buffalo, NY, USA, 1963.

[7] Bland, S. R. and Bennett, R. M. Wind-Tunnel Measurement of Propeller Whirl-Flutter Speeds and Static Stability Derivatives and Comparison with Theory, *NASA, TN D-1807*, 1963.

[8] Bennett, R. M. and Bland, S. R. Experimental and Analytical Investigation of Propeller Whirl Flutter of a Power Plant on a Flexible Wing, *NASA, TN D-2399*, 1964.

[9] Abbott, F.T., Jr., Kelly, H. N. and Hampton, K. D. Investigation of Propeller-Power Plant Autoprecession Boundaries for a Dynamic-Aeroelastic Model of a Four-Engine Turboprop Transport Airplane, *NASA, TN D-1806*, 1963.

[10] Kvaternik, R. G. and Kohn, J. S. An Experimental and Analytical Investigation of Proprotor Whirl Flutter, *NASA, TP 1047*, 1977.

[11] Krishna Rao, K. V. and Sundararajan, D. Whirl Flutter of Flapping Blade Rotor Systems, *National Aeronautical Laboratory*, Bangalore, India, TN-18, 1969.

[12] Čečrdle, J. Whirl Flutter of Turboprop Aircraft Structures, 2nd Ed., *Elsevier Science*, Oxford, UK, 2023.

[13] Maleček, J., Hlavatý, V., Malínek, P. and Čečrdle, J. Development of Wing / Engine Component Non-linear Aeroelastic Demonstrator, *In: International Forum on Aeroelasticity and Structural Dynamics*, Paris, France, 2011.

[14] Maleček, J., Čečrdle, J., Hlavatý, V. and Malínek, P. Mechanical Concepts for Simulation of Nonlinearities on Aeroelastic Demonstrator, *J. Aircr.*, 2013, 50(2):651-658.

[15] Čečrdle, J. and Maleček, J. Mechanical Concept of W-WING Whirl Flutter Aeroelastic Demonstrator, *Proc. Institution of Mech. Engineers, Part G: J. Aerosp. Eng.*, 2013, 229(8):1485-1494.

[16] Čečrdle, J., Malínek, P. and Vích, O. Wind Tunnel Test of a Whirl Flutter Aeroelastic Demonstrator, *In: Proc. AIAA SciTech Forum*, San Diego, CA, USA, 2017.

[17] Čečrdle, J., Vích, O. and Malínek, P. Wind Tunnel Test of a Whirl Flutter Aeroelastic Demonstrator, *Proc. Institution of Mech. Engineers, Part G: J. Aerosp. Eng.*, 2019, 233(3):969-977.

[18] Houbolt, J. C. and Reed, W. H. Propeller Nacelle Whirl Flutter, *J. Aerosp. Sci.*, 1962, 29:333-346.

[19] Dugeai, A., Mauffrey, Y. and Sicot, F. Aeroelastic Capabilities of the elsA Solver for Rotating Machines Applications, *In: Int. Forum on Aeroelasticity and Structural Dynamics*, Paris, France, 2011.

[20] Sicot, F. and Dugeai, A. Numerical Investigation of Propellers Whirl Flutter Using elsA, *In: Int. Forum on Aeroelasticity and Structural Dynamics*, Paris, France, 2011.

COPYRIGHT STATEMENT